

Nano Hexapod - Optimal Geometry

Dehaeze Thomas

April 2, 2025

Contents

1	Review of Stewart platforms	4
2	Effect of geometry on Stewart platform properties	7
2.1	Platform Mobility / Workspace	7
2.2	Stiffness	9
2.3	Dynamical properties	10
3	The Cubic Architecture	12
3.1	Static Properties	13
3.2	Dynamical Decoupling	15
3.3	Decentralized Control	17
3.4	Cubic architecture with Cube's center above the top platform	20
4	Nano Hexapod	24
4.1	Requirements	24
4.2	Obtained Geometry	24
4.3	Required Actuator stroke	25
4.4	Required Joint angular stroke	26
5	Conclusion	27
	Bibliography	28

The performance of a Stewart platform depends on its geometric configuration, especially the orientation of its struts and the positioning of its joints. During the conceptual design phase of the nano-hexapod, a preliminary geometry was selected based on general principles without detailed optimization. As the project advanced to the detailed design phase, a rigorous analysis of how geometry influences system performance became essential to ensure that the final design would meet the demanding requirements of the Nano Active Stabilization System (NASS).

In this chapter, the nano-hexapod geometry is optimized through careful analysis of how design parameters influence critical performance aspects: attainable workspace, mechanical stiffness, strut-to-strut coupling for decentralized control strategies, and dynamic response in Cartesian coordinates.

The chapter begins with a comprehensive review of existing Stewart platform designs in Section 1, surveying various approaches to geometry, actuation, sensing, and joint design from the literature. Section 2 develops the analytical framework that connects geometric parameters to performance characteristics, establishing quantitative relationships that guide the optimization process. Section 3 examines the cubic configuration a specialized architecture that has garnered significant attention for its purported advantages—to evaluate its suitability for the nano-hexapod application. Finally, Section 4 presents the optimized nano-hexapod geometry derived from these analyses and demonstrates how it addresses the specific requirements of the NASS.

1 Review of Stewart platforms

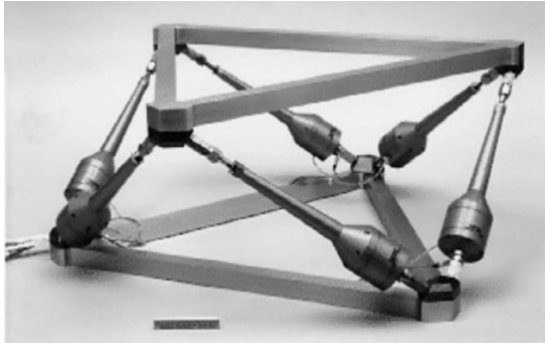
As was explained in the conceptual phase, Stewart platforms have the following key elements: two plates connected by six struts, with each strut composed of a joint at each end, an actuator, and one or several sensors. The exact geometry (i.e., position of joints and orientation of the struts) can be chosen freely depending on the application, which results in many different designs found in the literature. The focus is here made on Stewart platforms for nano-positioning and vibration control. Long stroke Stewart platforms are not considered here as their design imposes other challenges. Some Stewart platforms found in the literature are listed in Table 1.1.

Table 1.1: Examples of Stewart platform developed. When not specifically indicated, sensors are included in the struts. All presented Stewart platforms are using flexible joints. The table is ordered by appearance in the literature

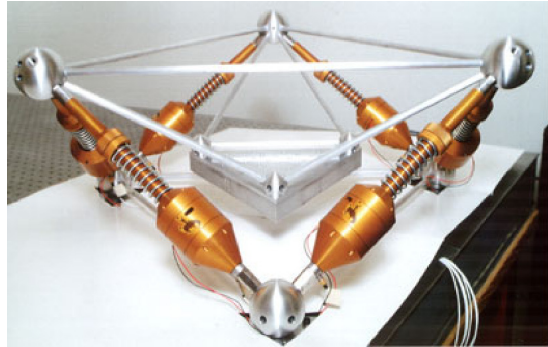
	Geometry	Actuators	Sensors	Reference
Figure 1.1a	Cubic	Magnetostrictive	Force, Accelerometers	[1]–[3]
	Cubic	Voice Coil (0.5 mm)	Force	[4], [5]
Figure 1.1b	Cubic	Voice Coil (10 mm)	Force, LVDT, Geophones	[6]–[8]
	Cubic	Voice Coil	Force	[9]–[13]
Figure 1.1c	Cubic	Piezoelectric (25 μm)	Force	[14]
	Cubic	APA (50 μm)	Force	[15]
Figure 1.2a	Non-Cubic	Voice Coil	Accelerometers	[16]
Figure 1.1d	Cubic	Voice Coil	Force	[17], [18]
	Cubic	Piezoelectric (50 μm)	Geophone	[19]
Figure 1.2b	Non-Cubic	Piezoelectric (16 μm)	Eddy Current	[20]
	Cubic	Piezoelectric (120 μm)	(External) Capacitive	[21], [22]
	Non-Cubic	Piezoelectric (160 μm)	(External) Capacitive	[23]
	Non-cubic	Magnetostrictive	Accelerometer	[24]
	Non-Cubic	Piezoelectric	Strain Gauge	[25]
Figure 1.2c	Cubic	Voice Coil	Accelerometer	[26]–[28]
	Cubic	Piezoelectric	Force	[29]
	Almost cubic	Voice Coil	Force, Accelerometer	[30], [31]
	Almost cubic	Piezoelectric	Force, Strain gauge	[32]
Figure 1.2d	Non-Cubic	3-phase rotary motor	Rotary Encoder	[33], [34]

All presented Stewart platforms utilize flexible joints, as this is a prerequisite for nano-positioning capabilities. Flexible joints can have various implementations, which will be discussed when designing the nano-hexapod flexible joints. In terms of actuation, most Stewart platforms employ either voice coil actuators (such as the ones shown in Figures 1.1a, 1.1b and 1.2a) or piezoelectric actuators (such as the ones shown in Figures 1.1c, 1.1d and 1.2c). Various sensors are integrated in the struts or on the plates depending on the application requirements. These include force sensors, inertial sensors, or relative displacement sensors. The actuator and sensor selection for the nano-hexapod will also be described in the next section.

There are two main categories of Stewart platform geometry. The first is cubic architecture (some exemplified are presented in Figure 1.1), where struts are positioned along six sides of a cube (and are therefore orthogonal to each other). Such specific architecture has some special properties that will be studied in Section 3. The second is non-cubic architecture (Figure 1.2), where the orientation of the struts and position of the joints can be optimized based on performance criteria. The effect of strut orientation and position of the joints on the Stewart platform properties is discussed Section 2.



(a) California Institute of Technology - USA



(b) University of Wyoming - USA

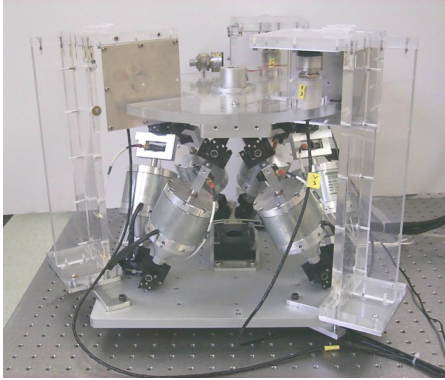


(c) ULB - Belgium



(d) Naval Postgraduate School - USA

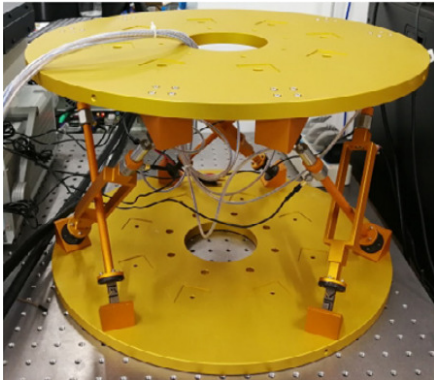
Figure 1.1: Some examples of developed Stewart platform with Cubic geometry. (a), (b), (c), (d)



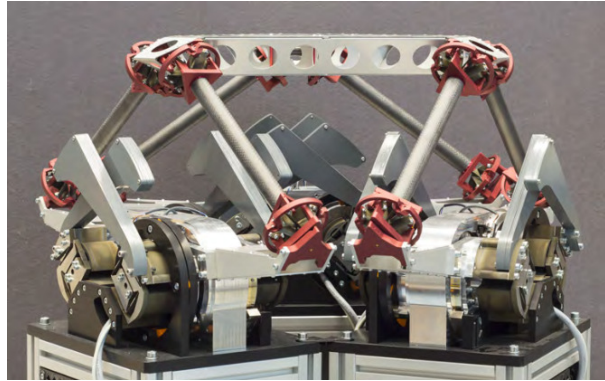
(a) Naval Postgraduate School - USA



(b) Beihang University - China



(c) Nanjing University - China



(d) University of Twente - Netherlands

Figure 1.2: Some examples of developed Stewart platform with non-cubic geometry. (a), (b), (c), (d)

2 Effect of geometry on Stewart platform properties

As was demonstrated during the conceptual phase, the geometry of the Stewart platform impacts the stiffness and compliance characteristics, the mobility or workspace, the force authority, and the dynamics of the manipulator. It is therefore essential to understand how the geometry impacts these properties, and to develop methodologies for optimizing the geometry for specific applications.

An important analytical tool for this study is the Jacobian matrix, which depends on \mathbf{b}_i (joint position with respect to the top platform) and $\hat{\mathbf{s}}_i$ (orientation of struts). The choice of frames ($\{A\}$ and $\{B\}$), independently of the physical Stewart platform geometry, impacts the obtained kinematics and stiffness matrix, as these are defined for forces and motion evaluated at the chosen frame.

2.1 Platform Mobility / Workspace

The mobility of the Stewart platform (or any manipulator) is defined as the range of motion that it can perform. It corresponds to the set of possible poses (i.e., combined translation and rotation) of frame $\{B\}$ with respect to frame $\{A\}$. This represents a six-dimensional property which is difficult to represent. Depending on the applications, only the translation mobility (i.e., fixed orientation workspace) or the rotation mobility may be represented. This approach is equivalent to projecting the six-dimensional value into a three-dimensional space, which is easier to represent.

Mobility of parallel manipulators is inherently difficult to study as the translational and orientation workspace are coupled [35]. The analysis is significantly simplified when considering small motions, as the Jacobian matrix can be used to link the strut motion to the motion of frame $\{B\}$ with respect to $\{A\}$ through (2.1), which is a linear equation.

$$\begin{bmatrix} \delta l_1 \\ \delta l_2 \\ \delta l_3 \\ \delta l_4 \\ \delta l_5 \\ \delta l_6 \end{bmatrix} = \begin{bmatrix} {}^A \hat{\mathbf{s}}_1^T & ({}^A \mathbf{b}_1 \times {}^A \hat{\mathbf{s}}_1)^T \\ {}^A \hat{\mathbf{s}}_2^T & ({}^A \mathbf{b}_2 \times {}^A \hat{\mathbf{s}}_2)^T \\ {}^A \hat{\mathbf{s}}_3^T & ({}^A \mathbf{b}_3 \times {}^A \hat{\mathbf{s}}_3)^T \\ {}^A \hat{\mathbf{s}}_4^T & ({}^A \mathbf{b}_4 \times {}^A \hat{\mathbf{s}}_4)^T \\ {}^A \hat{\mathbf{s}}_5^T & ({}^A \mathbf{b}_5 \times {}^A \hat{\mathbf{s}}_5)^T \\ {}^A \hat{\mathbf{s}}_6^T & ({}^A \mathbf{b}_6 \times {}^A \hat{\mathbf{s}}_6)^T \end{bmatrix} \begin{bmatrix} \delta x \\ \delta y \\ \delta z \\ \delta \theta_x \\ \delta \theta_y \\ \delta \theta_z \end{bmatrix} \quad (2.1)$$

Therefore, the mobility of the Stewart platform (defined as the set of achievable $[\delta x \ \delta y \ \delta z \ \delta \theta_x \ \delta \theta_y \ \delta \theta_z]$) depends on two key factors: the stroke of each strut and the geometry of the Stewart platform (embodied in the Jacobian matrix). More specifically, the XYZ mobility only depends on the s_i (orientation of struts), while the mobility in rotation also depends on b_i (position of top joints).

Mobility in translation For simplicity, only translations are first considered (i.e., fixed orientation of the Stewart platform). In the general case, the translational mobility can be represented by a 3D shape having 12 faces, where each actuator limits the stroke along its axis in positive and negative directions. The faces are therefore perpendicular to the strut direction. The obtained mobility for the Stewart platform geometry shown in Figure 2.1a is computed and represented in Figure 2.1b.

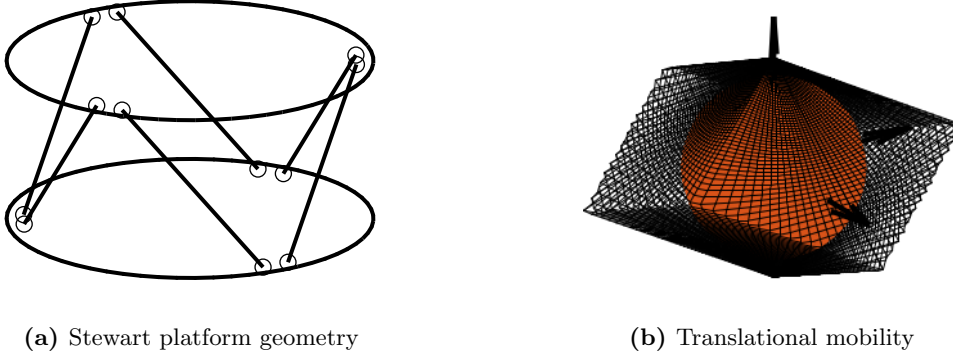


Figure 2.1: Example of one Stewart platform (a) and associated translational mobility (b)

With the previous interpretations of the 12 faces making the translational mobility 3D shape, it can be concluded that for a strut stroke of $\pm d$, a sphere with radius d is contained in the 3D shape and touches it along the six lines defined by the strut axes, as illustrated in Figure 2.1b. This means that the mobile platform can be translated in any direction with a stroke of d .

To better understand how the geometry of the Stewart platform impacts the translational mobility, two configurations are compared with struts oriented vertically (Figure 2.2a) and struts oriented horizontally (Figure 2.2b). The vertically oriented struts lead to greater stroke in the horizontal direction and reduced stroke in the vertical direction (Figure 2.2c). Conversely, horizontal oriented struts provide more stroke in the vertical direction.

It may seem counterintuitive that less stroke is available in the direction of the struts. This phenomenon occurs because the struts form a lever mechanism that amplifies the motion. The amplification factor increases when the struts have a high angle with the direction of motion and equals one when aligned with the direction of motion.

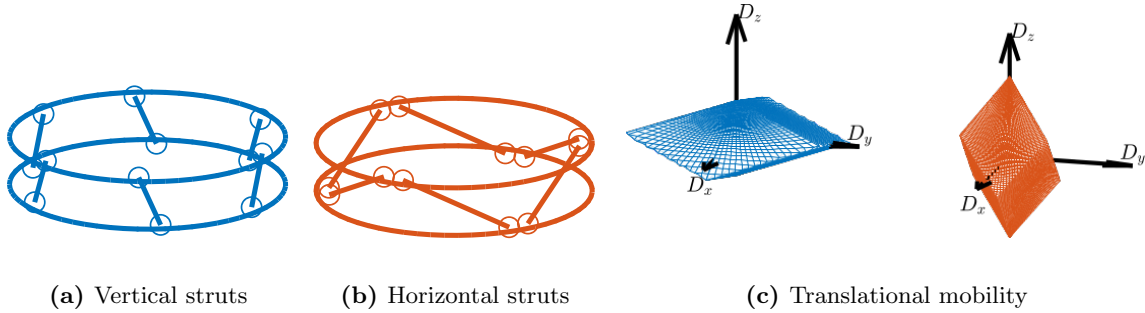


Figure 2.2: Effect of strut orientation on the obtained mobility in translation. Two Stewart platform geometry are considered: struts oriented vertically (a) and struts oriented horizontally (b). Obtained mobility for both geometry are shown in (c).

Mobility in rotation As shown by equation (2.1), the rotational mobility depends both on the orientation of the struts and on the location of the top joints. Similarly to the translational case, to increase

the rotational mobility in one direction, it is advantageous to have the struts more perpendicular to the rotational direction.

For instance, having the struts more vertical (Figure 2.2a) provides less rotational stroke along the vertical direction than having the struts oriented more horizontally (Figure 2.2b).

Two cases are considered with the same strut orientation but with different top joint positions: struts positioned close to each other (Figure 2.3a) and struts positioned further apart (Figure 2.3b). The mobility for pure rotations is compared in Figure 2.3c. Having struts further apart decreases the “lever arm” and therefore reduces the rotational mobility.

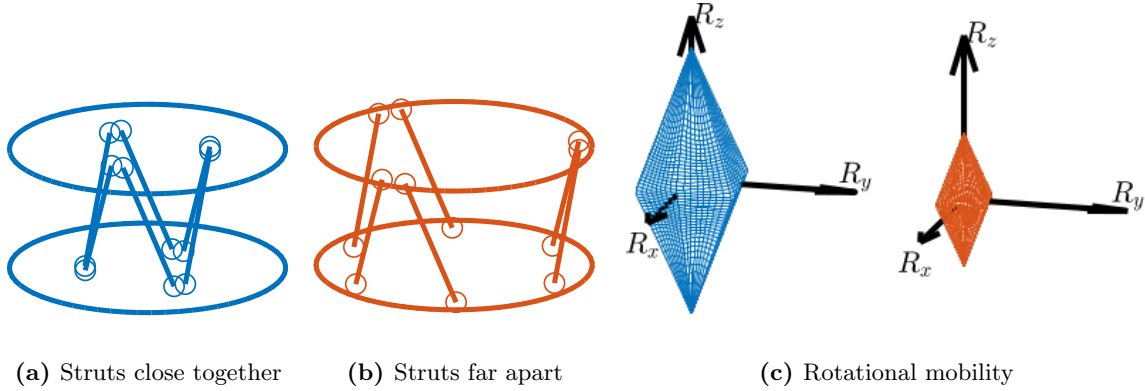


Figure 2.3: Effect of strut position on the obtained mobility in rotation. Two Stewart platform geometry are considered: struts close to each other (a) and struts further apart (b). Obtained mobility for both geometry are shown in (c).

Combined translations and rotations It is possible to consider combined translations and rotations, although displaying such mobility becomes more complex. For a fixed geometry and a desired mobility (combined translations and rotations), it is possible to estimate the required minimum actuator stroke. This analysis was conducted in Section 4 to estimate the required actuator stroke for the nano-hexapod geometry.

2.2 Stiffness

The stiffness matrix defines how the nano-hexapod deforms (frame $\{B\}$ with respect to frame $\{A\}$) due to static forces/torques applied on $\{B\}$. It depends on the Jacobian matrix (i.e., the geometry) and the strut axial stiffness as shown in equation (2.2). The contribution of joints stiffness is not considered here, as there were optimized after the geometry was fixed, but several work were done to quantify the impact of the flexible joint stiffness [11], [36].

$$\mathbf{K} = \mathbf{J}^T \mathbf{\mathcal{K}} \mathbf{J} \quad (2.2)$$

It is assumed that the stiffness of all struts is the same: $\mathbf{\mathcal{K}} = k \cdot \mathbf{I}_6$. In that case, the obtained stiffness matrix linearly depends on the strut stiffness k , and is structured as shown in equation (2.3).

$$\mathbf{K} = k\mathbf{J}^T\mathbf{J} = k \left[\begin{array}{c|c} \sum_{i=0}^6 \hat{\mathbf{s}}_i \cdot \hat{\mathbf{s}}_i^T & \sum_{i=0}^6 \hat{\mathbf{s}}_i \cdot ({}^A\mathbf{b}_i \times {}^A\hat{\mathbf{s}}_i)^T \\ \hline \sum_{i=0}^6 ({}^A\mathbf{b}_i \times {}^A\hat{\mathbf{s}}_i) \cdot \hat{\mathbf{s}}_i^T & \sum_{i=0}^6 ({}^A\mathbf{b}_i \times {}^A\hat{\mathbf{s}}_i) \cdot ({}^A\mathbf{b}_i \times {}^A\hat{\mathbf{s}}_i)^T \end{array} \right] \quad (2.3)$$

Translation Stiffness As shown by equation (2.3), the translation stiffnesses (the 3×3 top left terms of the stiffness matrix) only depend on the orientation of the struts and not their location: $\hat{\mathbf{s}}_i \cdot \hat{\mathbf{s}}_i^T$. In the extreme case where all struts are vertical with $s_i = [0, 0, 1]$, a vertical stiffness of $6k$ is achieved, but with null stiffness in the X and Y directions. If two struts are aligned along the X axis, two struts along the Y axis, and two struts along the Z axis, then $\hat{\mathbf{s}}_i \cdot \hat{\mathbf{s}}_i^T = 2\mathbf{I}_3$, resulting in well-distributed stiffness along all directions. This configuration corresponds to the cubic architecture presented in Section 3.

When struts are oriented more vertically (Figure 2.2a), vertical stiffness increases while horizontal stiffness decreases. Additionally, R_x and R_y stiffness increases while R_z stiffness decreases. The opposite conclusions apply if struts are oriented more horizontally (Figure 2.2b).

Rotational Stiffness The rotational stiffnesses depend both on the orientation of the struts and on the location of the top joints (with respect to the considered center of rotation, i.e., the location of frame $\{B\}$). With the same orientation but increased distances (b_i) by a factor of 2, the rotational stiffness is increased by a factor of 4. Therefore, the compact Stewart platform depicted in Figure 2.3a has less rotational stiffness than the Stewart platform shown in Figure 2.3b.

Diagonal Stiffness Matrix Having a diagonal stiffness matrix \mathbf{K} can be beneficial for control purposes as it would make the plant in the Cartesian frame decoupled at low frequency. This property depends on both the geometry and the chosen $\{B\}$ frame. For specific geometry and choice of $\{B\}$ frame, it is possible to achieve a diagonal K matrix. This is discussed in Section 3.1.

2.3 Dynamical properties

The dynamical equations (both in the Cartesian frame and in the frame of the struts) for the Stewart platform were derived during the conceptual phase with simplifying assumptions (massless struts and perfect joints). The dynamics depend both on the geometry (Jacobian matrix) and on the payload being placed on top of the platform. Under very specific conditions, the equations of motion in the Cartesian frame, given by equation (2.4), can be decoupled. These conditions are studied in Section 3.2.

$$\frac{\mathcal{X}}{\mathcal{F}}(s) = (\mathbf{M}s^2 + \mathbf{J}^T\mathbf{C}\mathbf{J}s + \mathbf{J}^T\mathbf{K}\mathbf{J})^{-1} \quad (2.4)$$

In the frame of the struts, the equations of motion given by equation (2.5) are well decoupled at low frequency. This is why most Stewart platforms are controlled in the frame of the struts: below the resonance frequency, the system is decoupled and SISO control may be applied for each strut, independently of the payload being used.

$$\frac{\mathcal{L}}{\mathcal{f}}(s) = (\mathbf{J}^{-T}\mathbf{M}\mathbf{J}^{-1}s^2 + \mathbf{C} + \mathbf{K})^{-1} \quad (2.5)$$

Coupling between sensors (force sensors, relative position sensors, inertial sensors) in different struts may also be important for decentralized control. In section 3.3, it will be studied whether the Stewart platform geometry can be optimized to have lower coupling between the struts.

Conclusion

The effects of two changes in the manipulator’s geometry, namely the position and orientation of the legs, are summarized in Table 2.1. These results could have been easily deduced based on mechanical principles, but thanks to the kinematic analysis, they can be quantified. These trade-offs provide important guidelines when choosing the Stewart platform geometry.

Table 2.1: Effect of a change in geometry on the manipulator’s stiffness, force authority and stroke

Struts	Vertically Oriented	Increased separation
Vertical stiffness	↗	=
Horizontal stiffness	↘	=
Vertical rotation stiffness	↘	↗
Horizontal rotation stiffness	↗	↗
Vertical stroke	↘	=
Horizontal stroke	↗	=
Vertical rotation stroke	↗	↘
Horizontal rotation stroke	↘	↘

3 The Cubic Architecture

The Cubic configuration for the Stewart platform was first proposed in [2]. This configuration is characterized by active struts arranged in a mutually orthogonal configuration connecting the corners of a cube, as shown in Figure 3.1a.

Typically, the struts have similar length to the cube's edges, as illustrated in Figure 3.1a. Practical implementations of such configurations can be observed in Figures 1.1a, 1.1b and 1.1d. It is also possible to implement designs with strut lengths smaller than the cube's edges (Figure 3.1b), as exemplified in Figure 1.1c.

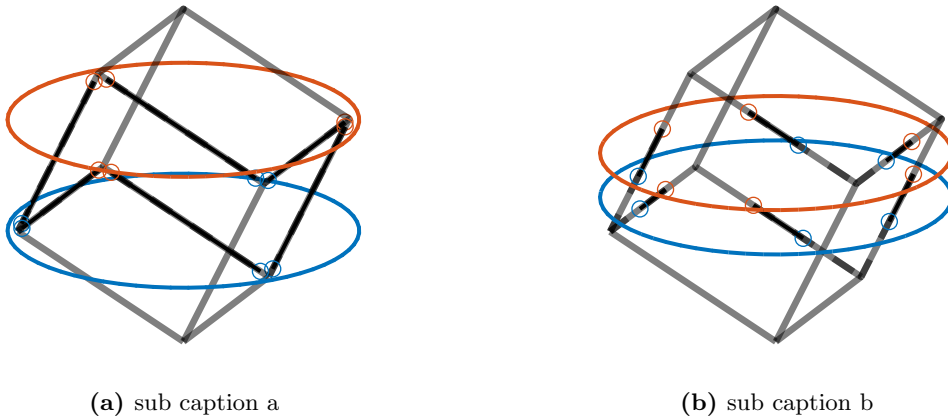


Figure 3.1: Typical Stewart platform cubic architectures. (a) (b)

Several advantageous properties attributed to the cubic configuration have contributed to its widespread adoption [2], [13], [18]: simplified kinematics relationships and dynamical analysis [2]; uniform stiffness in all directions [17]; uniform mobility [37, chapt.8.5.2]; and minimization of the cross coupling between actuators and sensors in different struts [18]. This minimization is attributed to the fact that the struts are orthogonal to each other, and is said to facilitate collocated sensor-actuator control system design, i.e., the implementation of decentralized control [2], [7].

These properties are examined in this section to assess their relevance for the nano-hexapod. The mobility and stiffness properties of the cubic configuration are analyzed in Section 3.1. Dynamical decoupling is investigated in Section 3.2, while decentralized control, crucial for the NASS, is examined in Section 3.3. Given that the cubic architecture imposes strict geometric constraints, alternative designs are proposed in Section 3.4. The ultimate objective is to determine the suitability of the cubic architecture for the nano-hexapod.

3.1 Static Properties

Stiffness matrix for the Cubic architecture Consider the cubic architecture depicted in Figure 3.2a. Consider the cubic architecture shown in Figure 3.2a. The unit vectors corresponding to the edges of the cube are described by equation (3.1).

$$\hat{s}_1 = \begin{bmatrix} \sqrt{2}/\sqrt{3} \\ 0 \\ 1/\sqrt{3} \end{bmatrix} \quad \hat{s}_2 = \begin{bmatrix} -1/\sqrt{6} \\ -1/\sqrt{2} \\ 1/\sqrt{3} \end{bmatrix} \quad \hat{s}_3 = \begin{bmatrix} -1/\sqrt{6} \\ 1/\sqrt{2} \\ 1/\sqrt{3} \end{bmatrix} \quad \hat{s}_4 = \begin{bmatrix} \sqrt{2}/\sqrt{3} \\ 0 \\ 1/\sqrt{3} \end{bmatrix} \quad \hat{s}_5 = \begin{bmatrix} -1/\sqrt{6} \\ -1/\sqrt{2} \\ 1/\sqrt{3} \end{bmatrix} \quad \hat{s}_6 = \begin{bmatrix} -1/\sqrt{6} \\ 1/\sqrt{2} \\ 1/\sqrt{3} \end{bmatrix} \quad (3.1)$$

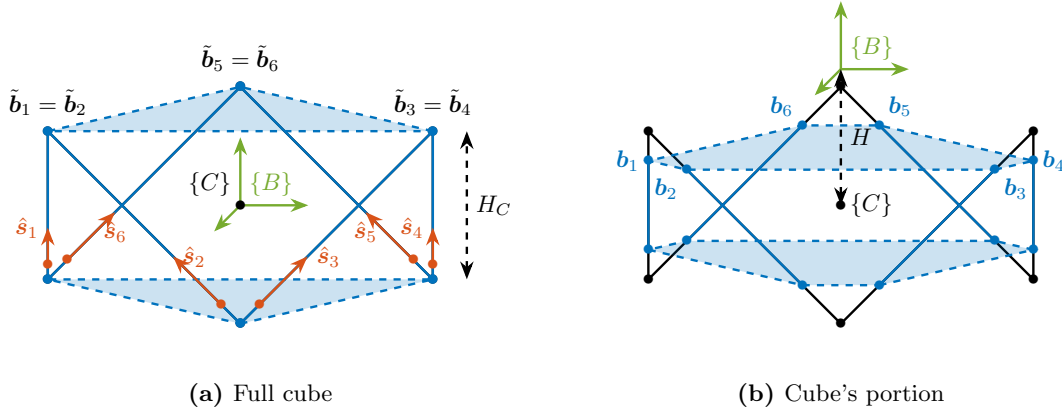


Figure 3.2: Cubic architecture. Struts are represented un blue. The cube's center by a black dot. The Struts can match the cube's edges (a) or just take a portion of the edge (b)

Coordinates of the cube's vertices relevant for the top joints, expressed with respect to the cube's center, are shown in equation (3.2).

$$\tilde{b}_1 = \tilde{b}_2 = H_c \begin{bmatrix} \frac{1}{\sqrt{2}} \\ \frac{-\sqrt{3}}{\sqrt{2}} \\ \frac{1}{2} \end{bmatrix}, \quad \tilde{b}_3 = \tilde{b}_4 = H_c \begin{bmatrix} \frac{1}{\sqrt{2}} \\ \frac{\sqrt{3}}{\sqrt{2}} \\ \frac{1}{2} \end{bmatrix}, \quad \tilde{b}_5 = \tilde{b}_6 = H_c \begin{bmatrix} \frac{-2}{\sqrt{2}} \\ 0 \\ \frac{1}{2} \end{bmatrix} \quad (3.2)$$

In the case where top joints are positioned at the cube's vertices, a diagonal stiffness matrix is obtained as shown in equation (3.3). Translation stiffness is twice the stiffness of the struts, and rotational stiffness is proportional to the square of the cube's size H_c .

$$\mathbf{K}_{\{B\}=\{C\}} = k \begin{bmatrix} 2 & 0 & 0 & 0 & 0 & 0 \\ 0 & 2 & 0 & 0 & 0 & 0 \\ 0 & 0 & 2 & 0 & 0 & 0 \\ 0 & 0 & 0 & \frac{3}{2}H_c^2 & 0 & 0 \\ 0 & 0 & 0 & 0 & \frac{3}{2}H_c^2 & 0 \\ 0 & 0 & 0 & 0 & 0 & 6H_c^2 \end{bmatrix} \quad (3.3)$$

However, typically, the top joints are not placed at the cube's vertices but at positions along the cube's edges (Figure 3.2b). In that case, the location of the top joints can be expressed by equation (3.4), yet

the computed stiffness matrix remains identical to Equation (3.3).

$$\mathbf{b}_i = \tilde{\mathbf{b}}_i + \alpha \hat{\mathbf{s}}_i \quad (3.4)$$

The stiffness matrix is therefore diagonal when the considered $\{B\}$ frame is located at the center of the cube (shown by frame $\{C\}$). This means that static forces (or torques) applied at the cube's center will induce pure translations (or rotations around the cube's center). This specific location where the stiffness matrix is diagonal is referred to as the "Center of Stiffness" (analogous to the "Center of Mass" where the mass matrix is diagonal).

Effect of having frame $\{B\}$ off-centered When the reference frames $\{A\}$ and $\{B\}$ are shifted from the cube's center, off-diagonal elements emerge in the stiffness matrix.

Considering a vertical shift as shown in Figure 3.2b, the stiffness matrix transforms into that shown in Equation (3.5). Off-diagonal elements increase proportionally with the height difference between the cube's center and the considered $\{B\}$ frame.

$$\mathbf{K}_{\{B\} \neq \{C\}} = k \begin{bmatrix} 2 & 0 & 0 & 0 & -2H & 0 \\ 0 & 2 & 0 & 2H & 0 & 0 \\ 0 & 0 & 2 & 0 & 0 & 0 \\ 0 & 2H & 0 & \frac{3}{2}H_c^2 + 2H^2 & 0 & 0 \\ -2H & 0 & 0 & 0 & \frac{3}{2}H_c^2 + 2H^2 & 0 \\ 0 & 0 & 0 & 0 & 0 & 6H_c^2 \end{bmatrix} \quad (3.5)$$

This stiffness matrix structure is characteristic of Stewart platforms exhibiting symmetry, and is not an exclusive property of cubic architectures. Therefore, the stiffness characteristics of the cubic architecture are only distinctive when considering a reference frame located at the cube's center. This poses a practical limitation, as in most applications, the relevant frame (where motion is of interest and forces are applied) is located above the top platform.

It should be noted that the cube's center need not be at the "center" of the Stewart platform. This can lead to interesting architectures shown in Section 3.4.

It should be noted that for the stiffness matrix to be diagonal, the cube's center need not coincide with the geometric center of the Stewart platform. This observation leads to the interesting alternative architectures presented in Section 3.4.

Uniform Mobility The translational mobility of the Stewart platform with constant orientation was analyzed. Considering limited actuator stroke (elongation of each strut), the maximum achievable positions in XYZ space were estimated. The resulting mobility in X, Y, and Z directions for the cubic architecture is illustrated in Figure 3.3a.

The translational workspace analysis reveals that for the cubic architecture, the achievable positions form a cube whose axes align with the struts, with the cube's edge length corresponding to the strut axial stroke. This findings suggest that the mobility pattern is more nuanced than sometimes described in the literature [11], exhibiting uniformity primarily along directions aligned with the cube's edges rather than uniform spherical distribution in all XYZ directions. This configuration still offers more

consistent mobility characteristics compared to alternative architectures illustrated in Figure 2.1. It is worth noting that the translational mobility properties remain independent of the cube’s size.

The rotational mobility, illustrated in Figure 3.3b, exhibit greater achievable angular displacements in the R_x and R_y directions compared to the R_z direction. Furthermore, an inverse relationship exists between the cube’s dimension and rotational mobility, with larger cube sizes corresponding to more limited angular displacement capabilities.

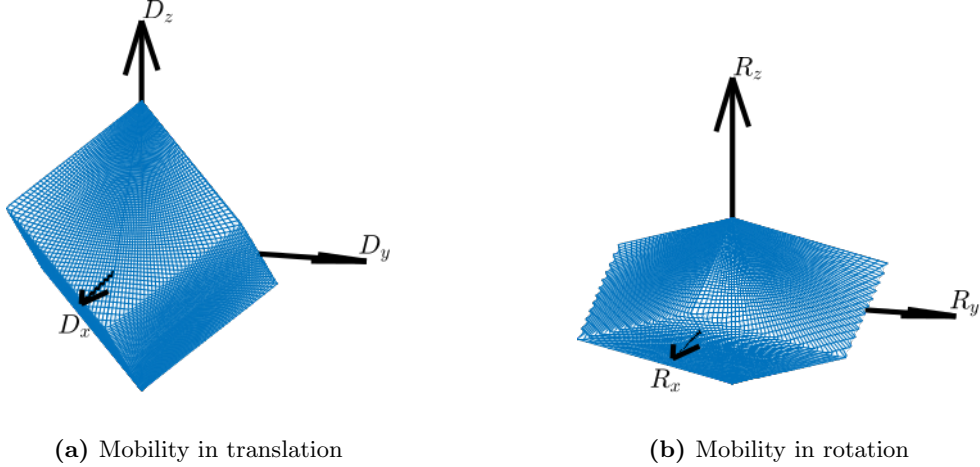


Figure 3.3: Mobility of a Stewart platform with Cubic architecture. Both for translations (a) and rotations (b)

3.2 Dynamical Decoupling

This section examines the dynamics of the cubic architecture in the Cartesian frame. This corresponds to the transfer function from forces and torques \mathcal{F} to translations and rotations \mathcal{X} of the top platform. When relative motion sensors are integrated in each strut (measuring \mathcal{L}), the pose \mathcal{X} is computed using the Jacobian matrix as shown in Figure 3.4.

The analysis aims to identify whether the cubic configuration exhibits special properties for control in the Cartesian frame.

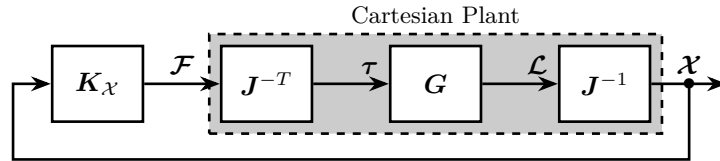


Figure 3.4: From Strut coordinate to Cartesian coordinate using the Jacobian matrix

Low frequency and High frequency coupling As derived during the conceptual design phase, the dynamics from \mathcal{F} to \mathcal{X} is described by Equation (?). At low frequency, the static behavior of the platform depends on the stiffness matrix (?). In Section 3.1, it was demonstrated that for the cubic configuration, the stiffness matrix is diagonal if frame $\{B\}$ is positioned at the cube’s center. In this case, the “Cartesian” plant is decoupled at low frequency. At high frequency, the behavior is governed

by the mass matrix (evaluated at frame $\{B\}$) (??). To achieve a diagonal mass matrix, the center of mass of the mobile components must coincide with the $\{B\}$ frame, and the principal axes of inertia must align with the axes of the $\{B\}$ frame.

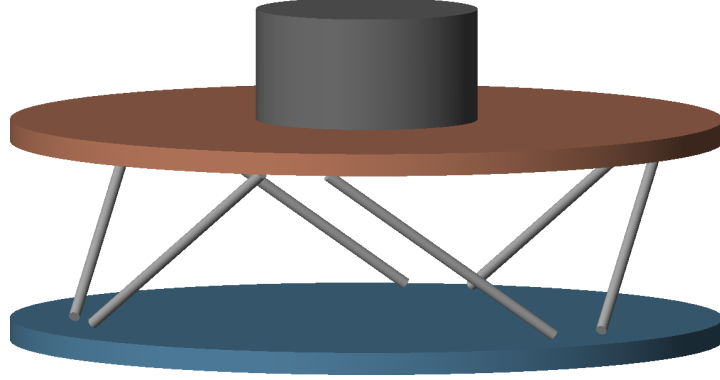


Figure 3.5: Cubic Stewart platform with top cylindrical payload

To verify these properties, a cubic Stewart platform with a cylindrical payload on top (Figure 3.5) was analyzed. Transfer functions from \mathcal{F} to \mathcal{X} were computed for two specific locations of the $\{B\}$ frames. When the $\{B\}$ frame was positioned at the center of mass, coupling at low frequency was observed due to the non-diagonal stiffness matrix (Figure 3.6a). Conversely, when positioned at the center of stiffness, coupling occurred at high frequency due to the non-diagonal mass matrix (Figure 3.6b).

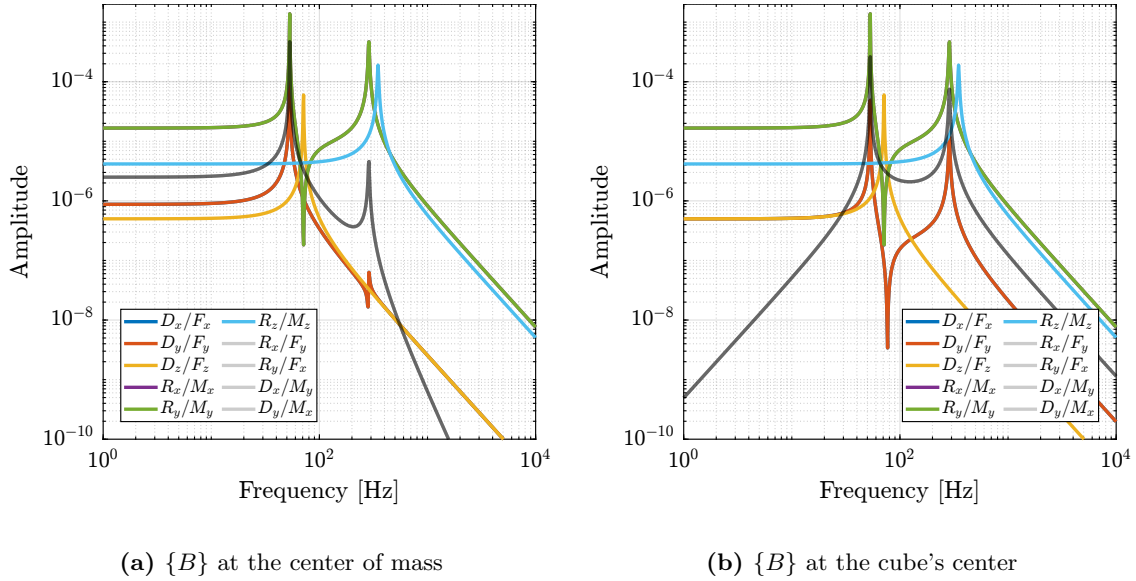


Figure 3.6: Transfer functions for a Cubic Stewart platform expressed in the Cartesian frame. Two locations of the $\{B\}$ frame are considered: at the cube's center (b) and at the center of mass of the moving body (a).

Payload's CoM at the cube's center An effective strategy for improving dynamical performances involves aligning the cube's center (center of stiffness) with the center of mass of the moving components [38]. This can be achieved by positioning the payload below the top platform, such that the center of mass of the moving body coincides with the cube's center (Figure 3.7a). This approach was physically

implemented in several studies [9], [13], as shown in Figure 1.1b. The resulting dynamics are indeed well-decoupled (Figure 3.7b), benefiting from simultaneously diagonal stiffness and mass matrices. The primary limitation of this approach is that, for many applications including the nano-hexapod, the payload must be positioned above the top platform. If a design similar to Figure 3.7a were employed for the nano-hexapod, the X-ray beam would intersect with the struts during spindle rotation.

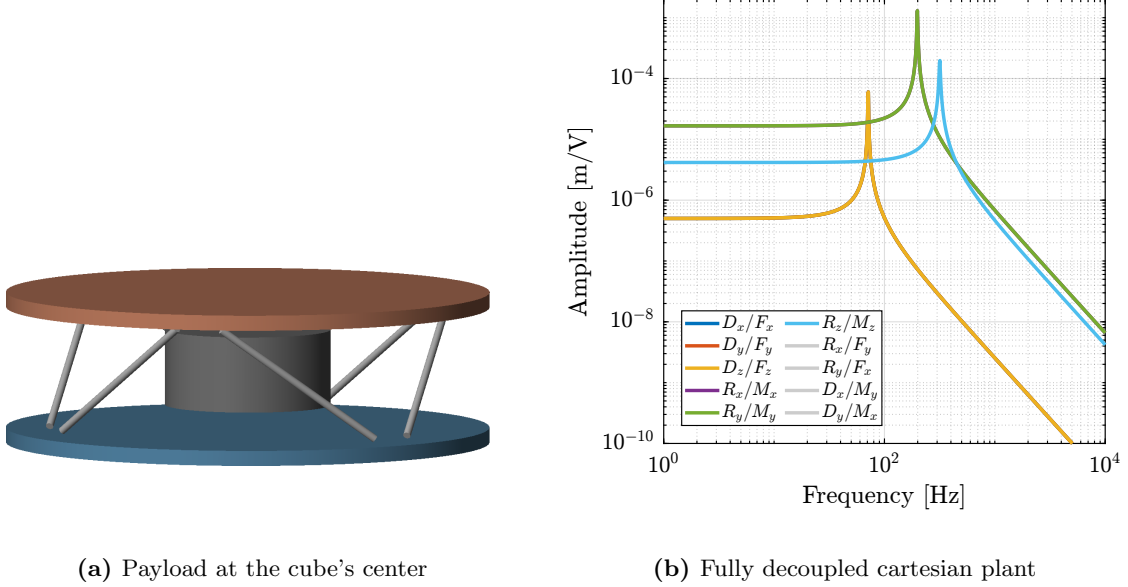


Figure 3.7: Cubic Stewart platform with payload at the cube's center (a). Obtained cartesian plant is fully decoupled (b)

Conclusion The analysis of dynamical properties of the cubic architecture yields several important conclusions. Static decoupling, characterized by a diagonal stiffness matrix, is achieved when reference frames $\{A\}$ and $\{B\}$ are positioned at the cube's center. This property can also be obtained with non-cubic architectures that exhibit symmetrical strut arrangements. Dynamic decoupling requires both static decoupling and coincidence of the mobile platform's center of mass with reference frame $\{B\}$. While this configuration offers powerful control advantages, it requires positioning the payload at the cube's center, which is highly restrictive and often impractical. Additionally, the cubic architecture provides uniform stiffness in XYZ directions, which may be advantageous for certain applications.

3.3 Decentralized Control

The orthogonal arrangement of struts in the cubic architecture suggests a potential minimization of inter-strut coupling, which could theoretically create favorable conditions for decentralized control. This section examines whether the cubic architecture actually demonstrates advantageous properties for decentralized control in the frame of the struts.

Two sensor types integrated in the struts are considered: displacement sensors and force sensors. The control architecture is illustrated in Figure 3.8, where $\mathbf{K}_{\mathcal{L}}$ represents a diagonal transfer function matrix.

The obtained plant dynamics in the frame of the struts are compared for two Stewart platforms. The

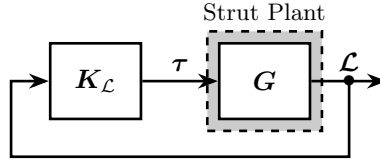


Figure 3.8: From Strut coordinate to Cartesian coordinate using the Jacobian matrix

first employs a cubic architecture shown in Figure 3.5. The second uses a non-cubic Stewart platform shown in Figure 3.9, featuring identical payload and strut dynamics but with struts oriented more vertically to differentiate it from the cubic architecture.

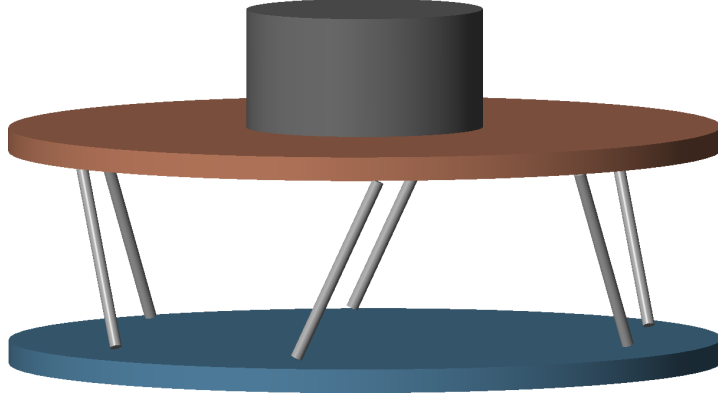


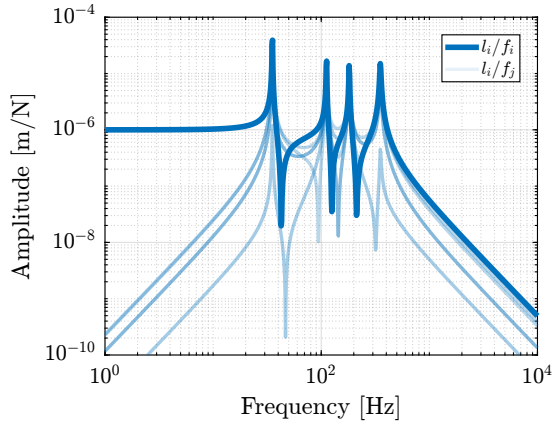
Figure 3.9: Stewart platform with non-cubic architecture

Relative Displacement Sensors The transfer functions from actuator force in each strut to the relative motion of the struts are presented in Figure 3.10. As anticipated from the equations of motion from \mathbf{f} to \mathcal{L} (2.5), the 6×6 plant is decoupled at low frequency. At high frequency, coupling is observed as the mass matrix projected in the strut frame is not diagonal.

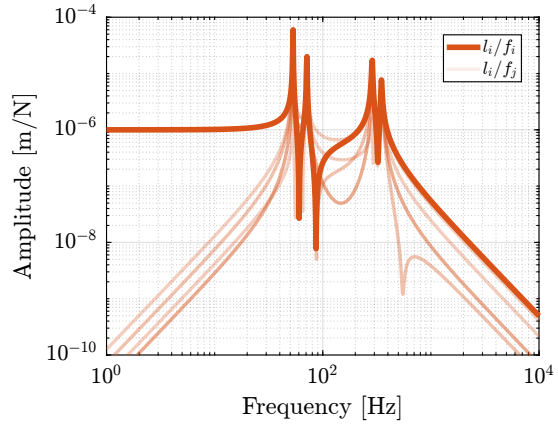
No significant advantage is evident for the cubic architecture (Figure 3.10b) compared to the non-cubic architecture (Figure 3.10a). The resonance frequencies differ between the two cases because the more vertical strut orientation in the non-cubic architecture alters the stiffness properties of the Stewart platform, consequently shifting the frequencies of various modes.

Force Sensors Similarly, the transfer functions from actuator force to force sensors in each strut were analyzed for both cubic and non-cubic Stewart platforms. The results are presented in Figure 3.11. The system demonstrates good decoupling at high frequency in both cases, with no evidence suggesting any advantage for the cubic architecture.

Conclusion The presented results do not demonstrate the pronounced decoupling advantages often associated with cubic architectures in the literature. Both the cubic and non-cubic configurations exhibited similar coupling characteristics in our modeling scenarios, suggesting that the benefits of orthogonal strut arrangement may be more nuanced than commonly described for decentralized control.

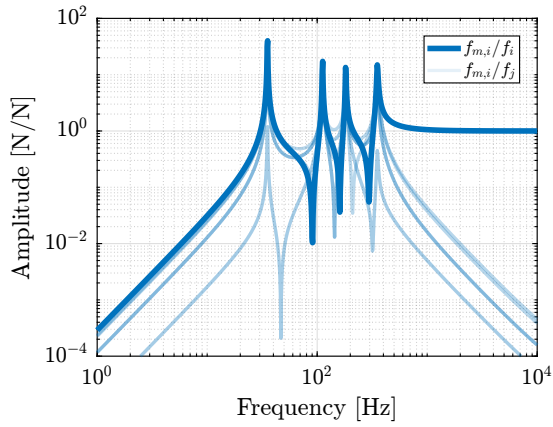


(a) Non cubic architecture

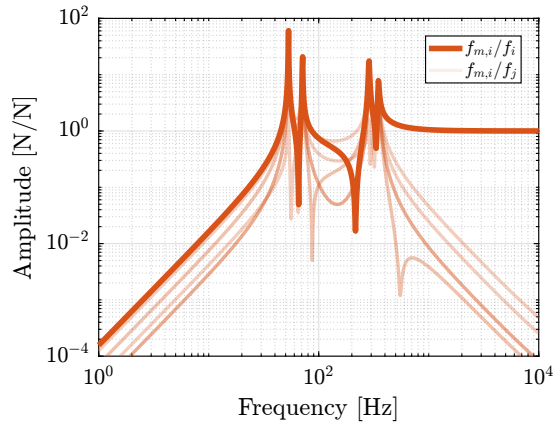


(b) Cubic architecture

Figure 3.10: Bode plot of the transfer functions from actuator force to relative displacement sensor in each strut. Both for a non-cubic architecture (a) and for a cubic architecture (b)



(a) Non cubic architecture



(b) Cubic architecture

Figure 3.11: Bode plot of the transfer functions from actuator force to force sensor in each strut. Both for a non-cubic architecture (a) and for a cubic architecture (b)

3.4 Cubic architecture with Cube's center above the top platform

As demonstrated in Section 3.2, the cubic architecture can exhibit advantageous dynamical properties when the center of mass of the moving body coincides with the cube's center, resulting in diagonal mass and stiffness matrices. As shown in Section 3.1, the stiffness matrix is diagonal when the considered $\{B\}$ frame is located at the cube's center. However, the $\{B\}$ frame is typically positioned above the top platform where forces are applied and displacements are measured.

This section proposes modifications to the cubic architecture to enable positioning the payload above the top platform while still leveraging the advantageous dynamical properties of the cubic configuration.

Three key parameters define the geometry of the cubic Stewart platform: H , the height of the Stewart platform (distance from fixed base to mobile platform); H_c , the height of the cube, as shown in Figure 3.2a; and H_{CoM} , the height of the center of mass relative to the mobile platform (coincident with the cube's center).

Depending on the cube's size H_c in relation to H and H_{CoM} , different designs emerge. In the following examples, $H = 100\text{ mm}$ and $H_{CoM} = 20\text{ mm}$.

Small cube When the cube size H_c is smaller than twice the height of the CoM H_{CoM} (3.6), the resulting design is shown in Figure 3.12.

$$H_c < 2H_{CoM} \quad (3.6)$$

This configuration is similar to that described in [20], although they do not explicitly identify it as a cubic configuration. Adjacent struts are parallel to each other, differing from the typical architecture where parallel struts are positioned opposite to each other.

This approach yields a compact architecture, but the small cube size may result in insufficient rotational stiffness.

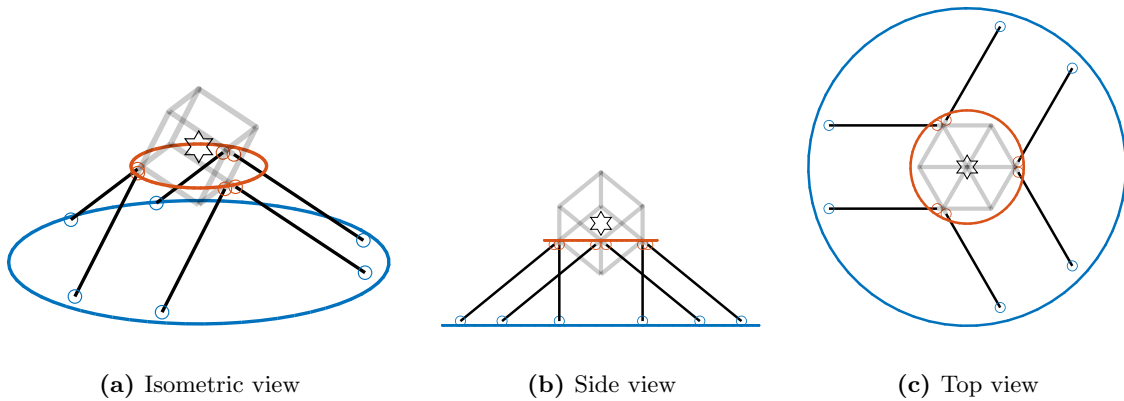


Figure 3.12: Cubic architecture with cube's center above the top platform. A cube height of 40mm is used.

Medium sized cube Increasing the cube's size such that (3.7) is verified produces an architecture with intersecting struts (Figure 3.13).

$$2H_{CoM} < H_c < 2(H_{CoM} + H) \quad (3.7)$$

This configuration resembles the design proposed in [32] (Figure 1.2c), although their design is not strictly cubic.

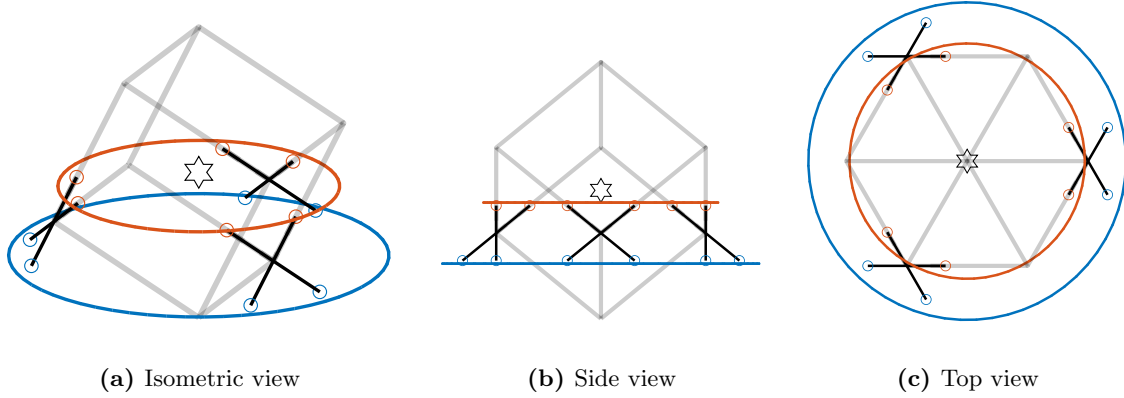


Figure 3.13: Cubic architecture with cube's center above the top platform. A cube height of 140mm is used.

Large cube When the cube's height exceeds twice the sum of the platform height and CoM height (3.8), the architecture shown in Figure 3.14 is obtained.

$$2(H_{CoM} + H) < H_c \quad (3.8)$$

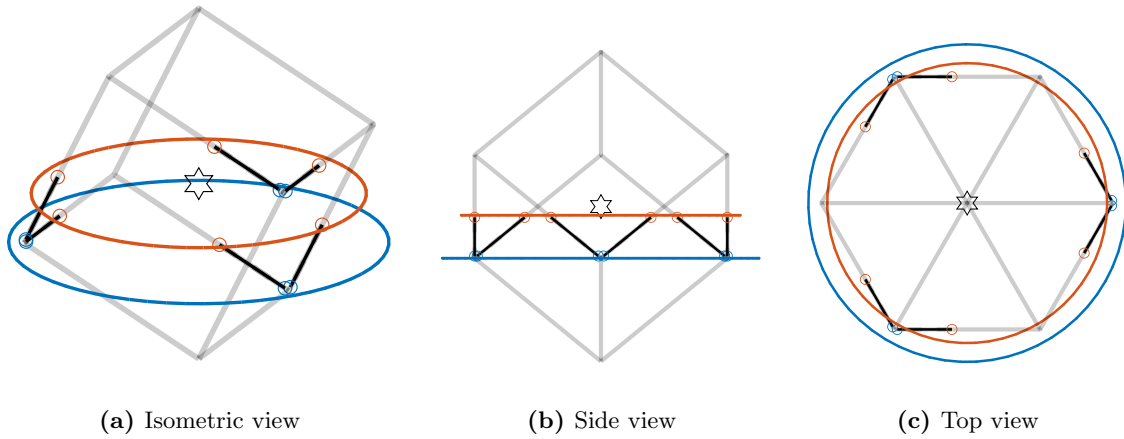


Figure 3.14: Cubic architecture with cube's center above the top platform. A cube height of 240mm is used.

Platform size In order to determine the approximate size of the platform as a function of For the proposed configuration, the top joints \mathbf{b}_i (resp. the bottom joints \mathbf{a}_i) and are positioned on a circle with radius R_{b_i} (resp. R_{a_i}) described by Equation (3.9).

$$R_{b_i} = \sqrt{\frac{3}{2}H_c^2 + 2H_{CoM}^2} \quad (3.9a)$$

$$R_{a_i} = \sqrt{\frac{3}{2}H_c^2 + 2(H_{CoM} + H)^2} \quad (3.9b)$$

Since the rotational stiffness for the cubic architecture scales with the square of the cube's height (3.3), the cube's size can be determined based on rotational stiffness requirements. Subsequently, using Equation (3.9), the dimensions of the top and bottom platforms can be calculated.

Conclusion The configurations proposed in this analysis represent derivations from the classical cubic architecture, wherein the cube's center is typically located at the Stewart platform's center. Three distinct configurations have been identified, each with different geometric arrangements but sharing the common characteristic that the cube's center is positioned above the top platform. This structural modification enables the alignment of the moving body's center of mass with the center of stiffness, resulting in beneficial decoupling properties in the Cartesian frame.

These proposed architectures maintain the fundamental advantages inherent to the cubic configuration, such as uniform stiffness and uniform mobility, while providing favorable dynamical properties when payloads are placed on top of the mobile platform. This approach allows for practical payload positioning while preserving the desirable control characteristics associated with the cubic architecture, making these configurations potentially useful for applications requiring both specific payload placement and good dynamic performance.

Conclusion

The analysis of the cubic architecture for Stewart platforms has yielded several important findings. While the cubic configuration provides uniform stiffness in the XYZ directions, its stiffness property becomes particularly advantageous when forces and torques are applied at the cube's center. Under these conditions, the stiffness matrix becomes diagonal, resulting in a decoupled Cartesian plant at low frequencies.

Regarding mobility, the translational capabilities of the cubic configuration exhibit uniformity along the directions of the orthogonal struts, rather than complete uniformity in the Cartesian space. This understanding refines the characterization of cubic architecture mobility commonly presented in literature.

The analysis of decentralized control in the frame of the struts revealed more nuanced results than expected. While cubic architectures are frequently associated with reduced coupling between actuators and sensors, our comparative study showed that these benefits may be more subtle or context-dependent than commonly described. Under the conditions analyzed, the coupling characteristics of cubic and non-cubic configurations appeared similar.

Fully decoupled dynamics can be achieved when the center of mass of the moving body coincides with the cube's center. However, this arrangement presents practical challenges, as the cube's center is traditionally located between the top and bottom platforms, making payload placement problematic for many applications.

To address this limitation, modified cubic architectures have been proposed with the cube's center positioned above the top platform. These configurations maintain the fundamental advantages of the cubic architecture while enabling practical payload placement.

4 Nano Hexapod

Based on previous analysis, this section aims to determine the nano-hexapod geometry.

For the NASS, the chosen reference frames $\{A\}$ and $\{B\}$ coincide with the sample's point of interest, which is positioned 150 mm above the top platform. This is the location where precise control of the sample's position is required, as it is where the x-ray beam is focused.

4.1 Requirements

The design of the nano-hexapod must satisfy several constraints. The device should fit within a cylinder with radius of 120 mm and height of 95 mm . Based on the measured errors of all stages of the micro-stations, and incorporating safety margins, the required mobility should enable combined translations in any direction of $\pm 50\text{ }\mu\text{m}$. At any position, the system should be capable of performing R_x and R_y rotations of $\pm 50\text{ }\mu\text{rad}$. Regarding stiffness, the resonance frequencies should be well above the maximum rotational velocity of $2\pi\text{ rad/s}$ to minimize gyroscopic effects, while remaining below the problematic modes of the micro-station to ensure decoupling from its complex dynamics. In terms of dynamics, the design should facilitate implementation of Integral Force Feedback (IFF) in a decentralized manner, and provide good decoupling for the high authority controller in the frame of the struts.

A significant challenge in optimizing the nano-hexapod design arises from the variety of payloads that will be used, with masses ranging from 1 to 50kg. This variation in payload characteristics makes it impossible to develop a single geometry that provides optimal dynamical properties for all possible configurations.

4.2 Obtained Geometry

Based on the previous analysis of Stewart platform configurations, while the geometry can be optimized to achieve the desired trade-off between stiffness and mobility in different directions, the wide range of potential payloads complicates the optimization process for obtaining consistent dynamical properties across all usage scenarios.

For the nano-hexapod design, the struts were oriented more vertically compared to a cubic architecture due to several important considerations. First, the requirements in the vertical direction are more stringent than in the horizontal direction. This vertical strut orientation decreases the amplification factor in the vertical direction, providing greater resolution and reducing the effects of actuator noise. Second, the micro-station's vertical modes exhibit higher frequencies than its lateral modes. Therefore, higher resonance frequencies of the nano-hexapod in the vertical direction compared to the horizontal direction enhance the decoupling properties between the micro-station and the nano-hexapod.

Regarding dynamic properties, particularly for control in the frame of the struts, no specific optimization was implemented since the analysis revealed that the particular geometry has minimal impact on the resulting coupling characteristics.

Consequently, the geometry was selected according to practical constraints. The height between the two plates is set at 95 mm . Both platforms utilize the maximum available size, with joints offset by 15 mm from the plate surfaces and positioned along circles with radii of 120 mm for the fixed joints and 110 mm for the mobile joints. The positioning angles, as shown in Figure 4.1b, are $[255, 285, 15, 45, 135, 165]$ degrees for the top joints and $[220, 320, 340, 80, 100, 200]$ degrees for the bottom joints.

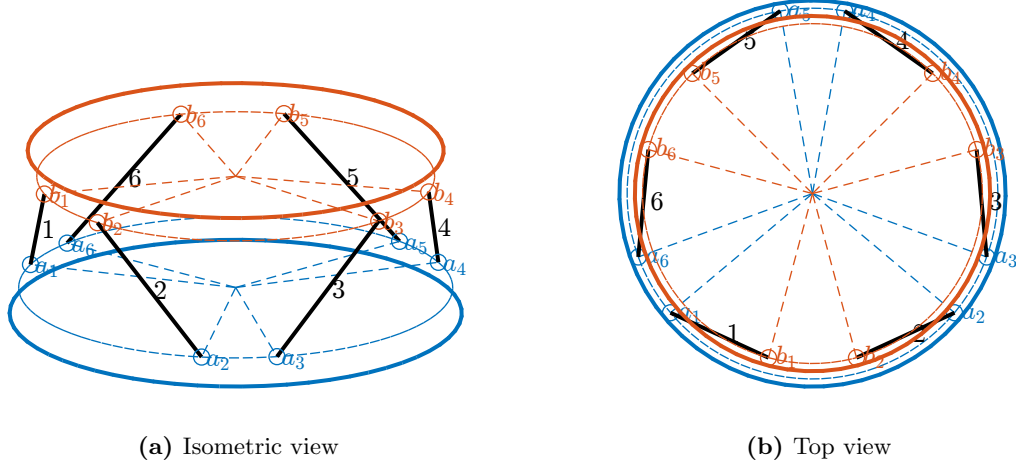


Figure 4.1: Obtained architecture for the Nano Hexapod

The resulting geometry is illustrated in Figure 4.1. While minor refinements may occur during detailed mechanical design to address manufacturing and assembly considerations, the fundamental geometry will remain consistent with this configuration. This geometry serves as the foundation for estimating required actuator stroke (Section 4.3), determining flexible joint stroke requirements (Section 4.4), performing noise budgeting for instrumentation selection, and developing control strategies. Implementing a cubic architecture as proposed in Section 3.4 was considered. However, positioning the cube's center 150 mm above the top platform would have resulted in platform dimensions exceeding the maximum available size. Additionally, to benefit from the cubic configuration's dynamical properties, each payload would require careful calibration of inertia before placement on the nano-hexapod, ensuring that its center of mass coincides with the cube's center. Given the impracticality of consistently aligning the center of mass with the cube's center, the cubic architecture was deemed unsuitable for the nano-hexapod application.

4.3 Required Actuator stroke

With the geometry established, the actuator stroke necessary to achieve the desired mobility can be determined.

The required mobility parameters include combined translations in the XYZ directions of $\pm 50\ \mu\text{m}$ (essentially a cubic workspace). Additionally, at any point within this workspace, combined R_x and R_y rotations of $\pm 50\ \mu\text{rad}$, with R_z maintained at 0, should be possible.

Calculations based on the selected geometry indicate that an actuator stroke of $\pm 94\ \mu\text{m}$ is required

to achieve the desired mobility. This specification will be used during the actuator selection process. Figure 4.2 illustrates both the desired mobility (represented as a cube) and the calculated mobility envelope of the nano-hexapod with an actuator stroke of $\pm 94 \mu m$. The diagram confirms that the required workspace fits within the system's capabilities.

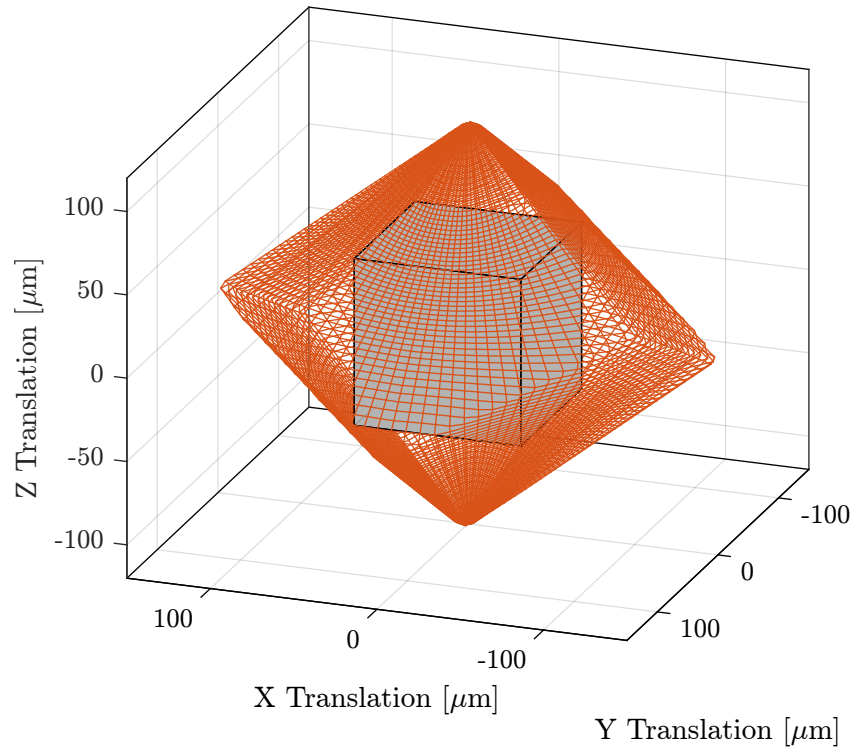


Figure 4.2: Wanted translation mobility of the Nano-Hexapod (grey cube) and computed Mobility (red volume).

4.4 Required Joint angular stroke

With the nano-hexapod geometry and mobility requirements established, the flexible joint angular stroke necessary to avoid limiting the achievable workspace can be determined.

This analysis focuses solely on bending stroke, as the torsional stroke of the flexible joints is expected to be minimal given the absence of vertical rotation requirements.

The required angular stroke for both fixed and mobile joints is calculated to be 1 mrad. This specification will guide the design of the flexible joints.

5 Conclusion

This chapter has explored the optimization of the nano-hexapod geometry for the Nano Active Stabilization System (NASS).

First, a review of existing Stewart platforms revealed two main geometric categories: cubic architectures, characterized by mutually orthogonal struts arranged along the edges of a cube, and non-cubic architectures with varied strut orientations. While cubic architectures are prevalent in the literature and attributed with beneficial properties such as simplified kinematics, uniform stiffness, and reduced cross-coupling, the performed analysis revealed that some of these advantages may be more nuanced or context-dependent than commonly described.

The analytical relationships between Stewart platform geometry and its mechanical properties were established, enabling a better understanding of the trade-offs between competing requirements such as mobility and stiffness along different axes. These insights were useful during the nano-hexapod geometry optimization.

For the cubic configuration, complete dynamical decoupling in the Cartesian frame can be achieved when the center of mass of the moving body coincides with the cube's center, but this arrangement is often impractical for real-world applications. Modified cubic architectures with the cube's center positioned above the top platform were proposed as a potential solution, but proved unsuitable for the nano-hexapod due to size constraints and the impracticality of ensuring that different payloads' centers of mass would consistently align with the cube's center.

For the nano-hexapod design, a key challenge was addressing the wide range of potential payloads (1 to 50kg), which made it impossible to optimize the geometry for consistent dynamic performance across all usage scenarios. This led to a practical design approach where struts were oriented more vertically than in cubic configurations to address several application-specific needs: achieving higher resolution in the vertical direction by reducing amplification factors, better matching the micro-station's modal characteristics with higher vertical resonance frequencies, and accommodating the stringent vertical positioning requirements.

Bibliography

- [1] Z. Geng and L. S. Haynes, “Six-degree-of-freedom active vibration isolation using a stewart platform mechanism,” *Journal of Robotic Systems*, vol. 10, no. 5, pp. 725–744, 1993 (cit. on p. 4).
- [2] Z. Geng and L. Haynes, “Six degree-of-freedom active vibration control using the stewart platforms,” *IEEE Transactions on Control Systems Technology*, vol. 2, no. 1, pp. 45–53, 1994 (cit. on pp. 4, 12).
- [3] Z. J. Geng, G. G. Pan, L. S. Haynes, B. K. Wada, and J. A. Garba, “An intelligent control system for multiple degree-of-freedom vibration isolation,” *Journal of Intelligent Material Systems and Structures*, vol. 6, no. 6, pp. 787–800, 1995 (cit. on p. 4).
- [4] J. Spanos, Z. Rahman, and G. Blackwood, “A soft 6-axis active vibration isolator,” in *Proceedings of 1995 American Control Conference - ACC’95*, 1995 (cit. on p. 4).
- [5] Z. H. Rahman, J. T. Spanos, and R. A. Laskin, “Multiaxis vibration isolation, suppression, and steering system for space observational applications,” in *Telescope Control Systems III*, May 1998 (cit. on p. 4).
- [6] D. Thayer and J. Vagners, “A look at the pole/zero structure of a stewart platform using special coordinate basis,” in *Proceedings of the 1998 American Control Conference. ACC (IEEE Cat. No.98CH36207)*, 1998 (cit. on p. 4).
- [7] D. Thayer, M. Campbell, J. Vagners, and A. von Flotow, “Six-axis vibration isolation system using soft actuators and multiple sensors,” *Journal of Spacecraft and Rockets*, vol. 39, no. 2, pp. 206–212, 2002 (cit. on pp. 4, 12).
- [8] G. Hauge and M. Campbell, “Sensors and control of a space-based six-axis vibration isolation system,” *Journal of Sound and Vibration*, vol. 269, no. 3-5, pp. 913–931, 2004 (cit. on p. 4).
- [9] J. McInroy, “Dynamic modeling of flexure jointed hexapods for control purposes,” in *Proceedings of the 1999 IEEE International Conference on Control Applications (Cat. No.99CH36328)*, 1999 (cit. on pp. 4, 17).
- [10] J. McInroy, J. O’Brien, and G. Neat, “Precise, fault-tolerant pointing using a stewart platform,” *IEEE/ASME Transactions on Mechatronics*, vol. 4, no. 1, pp. 91–95, 1999 (cit. on p. 4).
- [11] J. McInroy and J. Hamann, “Design and control of flexure jointed hexapods,” *IEEE Transactions on Robotics and Automation*, vol. 16, no. 4, pp. 372–381, 2000 (cit. on pp. 4, 9, 14).
- [12] X. Li, J. C. Hamann, and J. E. McInroy, “Simultaneous vibration isolation and pointing control of flexure jointed hexapods,” in *Smart Structures and Materials 2001: Smart Structures and Integrated Systems*, Aug. 2001 (cit. on p. 4).
- [13] F. Jafari and J. McInroy, “Orthogonal gough-stewart platforms for micromanipulation,” *IEEE Transactions on Robotics and Automation*, vol. 19, no. 4, pp. 595–603, Aug. 2003 (cit. on pp. 4, 12, 17).
- [14] A. Defendini, L. Vaillon, F. Trouve, *et al.*, “Technology predevelopment for active control of vibration and very high accuracy pointing systems,” in *Spacecraft Guidance, Navigation and Control Systems*, vol. 425, 2000, p. 385 (cit. on p. 4).

- [15] A. Abu Hanieh, M. Horodinca, and A. Preumont, “Stiff and soft stewart platforms for active damping and active isolation of vibrations,” in *Actuator 2002, 8th International Conference on New Actuators*, 2002 (cit. on p. 4).
- [16] H.-J. Chen, R. Bishop, and B. Agrawal, “Payload pointing and active vibration isolation using hexapod platforms,” in *44th AIAA/ASME/ASCE/AHS/ASC Structures, Structural Dynamics, and Materials Conference*, Apr. 2003 (cit. on p. 4).
- [17] A. A. Hanieh, “Active isolation and damping of vibrations via stewart platform,” Ph.D. dissertation, Université Libre de Bruxelles, Brussels, Belgium, 2003 (cit. on pp. 4, 12).
- [18] A. Preumont, M. Horodinca, I. Romanescu, *et al.*, “A six-axis single-stage active vibration isolator based on stewart platform,” *Journal of Sound and Vibration*, vol. 300, no. 3-5, pp. 644–661, 2007 (cit. on pp. 4, 12).
- [19] B. N. Agrawal and H.-J. Chen, “Algorithms for active vibration isolation on spacecraft using a stewart platform,” *Smart Materials and Structures*, vol. 13, no. 4, pp. 873–880, 2004 (cit. on p. 4).
- [20] K. Furutani, M. Suzuki, and R. Kudoh, “Nanometre-cutting machine using a stewart-platform parallel mechanism,” *Measurement Science and Technology*, vol. 15, no. 2, pp. 467–474, 2004 (cit. on pp. 4, 20).
- [21] Y. Ting, H.-C. Jar, and C.-C. Li, “Design of a 6dof stewart-type nanoscale platform,” in *2006 Sixth IEEE Conference on Nanotechnology*, 2006 (cit. on p. 4).
- [22] Y. Ting, C.-C. Li, and T. V. Nguyen, “Composite controller design for a 6dof stewart nanoscale platform,” *Precision Engineering*, vol. 37, no. 3, pp. 671–683, 2013 (cit. on p. 4).
- [23] Y. Ting, H.-C. Jar, and C.-C. Li, “Measurement and calibration for stewart micromanipulation system,” *Precision Engineering*, vol. 31, no. 3, pp. 226–233, 2007 (cit. on p. 4).
- [24] Z. Zhang, J. Liu, J. Mao, Y. Guo, and Y. Ma, “Six dof active vibration control using stewart platform with non-cubic configuration,” in *2011 6th IEEE Conference on Industrial Electronics and Applications*, Jun. 2011 (cit. on p. 4).
- [25] Z. Du, R. Shi, and W. Dong, “A piezo-actuated high-precision flexible parallel pointing mechanism: Conceptual design, development, and experiments,” *IEEE Transactions on Robotics*, vol. 30, no. 1, pp. 131–137, 2014 (cit. on p. 4).
- [26] W. Chi, D. Cao, D. Wang, *et al.*, “Design and experimental study of a vcm-based stewart parallel mechanism used for active vibration isolation,” *Energies*, vol. 8, no. 8, pp. 8001–8019, 2015 (cit. on p. 4).
- [27] J. Tang, D. Cao, and T. Yu, “Decentralized vibration control of a voice coil motor-based stewart parallel mechanism: Simulation and experiments,” *Proceedings of the Institution of Mechanical Engineers, Part C: Journal of Mechanical Engineering Science*, vol. 233, no. 1, pp. 132–145, 2018 (cit. on p. 4).
- [28] J. Jiao, Y. Wu, K. Yu, and R. Zhao, “Dynamic modeling and experimental analyses of stewart platform with flexible hinges,” *Journal of Vibration and Control*, vol. 25, no. 1, pp. 151–171, 2018 (cit. on p. 4).
- [29] C. Wang, X. Xie, Y. Chen, and Z. Zhang, “Investigation on active vibration isolation of a stewart platform with piezoelectric actuators,” *Journal of Sound and Vibration*, vol. 383, pp. 1–19, Nov. 2016 (cit. on p. 4).
- [30] M. Beijen, M. Heertjes, J. V. Dijk, and W. Hakvoort, “Self-tuning mimo disturbance feedforward control for active hard-mounted vibration isolators,” *Control Engineering Practice*, vol. 72, pp. 90–103, 2018 (cit. on p. 4).
- [31] D. Tjepkema, “Active hard mount vibration isolation for precision equipment [ph. d. thesis],” Ph.D. dissertation, 2012 (cit. on p. 4).

- [32] X. Yang, H. Wu, B. Chen, S. Kang, and S. Cheng, “Dynamic modeling and decoupled control of a flexible stewart platform for vibration isolation,” *Journal of Sound and Vibration*, vol. 439, pp. 398–412, Jan. 2019 (cit. on pp. 4, 21).
- [33] M. Naves, “Design and optimization of large stroke flexure mechanisms,” Ph.D. dissertation, Univeristy of Twente, 2020 (cit. on p. 4).
- [34] M. Naves, W. Hakvoort, M. Nijenhuis, and D. Brouwer, “T-flex: A large range of motion fully flexure-based 6-dof hexapod,” in *20th EUSPEN International Conference & Exhibition, EUSPEN 2020*, EUSPEN, 2020, pp. 205–208 (cit. on p. 4).
- [35] J.-P. Merlet, “Still a long way to go on the road for parallel mechanisms,” in *Proc. ASME 2002 DETC Conf., Montreal, 2002* (cit. on p. 7).
- [36] J. McInroy, “Modeling and design of flexure jointed stewart platforms for control purposes,” *IEEE/ASME Transactions on Mechatronics*, vol. 7, no. 1, pp. 95–99, 2002 (cit. on p. 9).
- [37] A. Preumont, *Vibration Control of Active Structures - Fourth Edition* (Solid Mechanics and Its Applications). Springer International Publishing, 2018 (cit. on p. 12).
- [38] X. Li, “Simultaneous, fault-tolerant vibration isolation and pointing control of flexure jointed hexapods,” Ph.D. dissertation, University of Wyoming, 2001 (cit. on p. 16).